Available online at www.sciencedirect.com

ScienceDirect

Mendeleev Commun., 2022, **32**, 323–326

Mendeleev Communications

Template synthesis of ε-Fe_2O_3 nanoparticles in opal-like matrices

Alexander I. Sharapaev,*[a] Aytan G. Muradova,[a] Nikolay P. Simonenko,[b] Valeriy M. Cherepanov,[c] Anton Yu. Yurenya[c] and Nikolay K. Chumakov[c]

[a] *D. I. Mendeleev University of Chemical Technology of Russia, 125047 Moscow, Russian Federation. E-mail: a.sharapaev@gmail.com*

[b] *N. S. Kurnakov Institute of General and Inorganic Chemistry, Russian Academy of Sciences, 119071 Moscow, Russian Federation*

[c] *National Research Center 'Kurchatov Institute', 123182 Moscow, Russian Federation*

DOI: 10.1016/j.mencom.2022.05.010

Nanoparticles of ε-Fe_2O_3 were obtained by template synthesis in the pores of opal-like matrices. The maximum content of ε-Fe_2O_3 is achieved upon calcination at 1000 °C for 2–4 h. The content of ε-Fe_2O_3 in a mixture of modifications of iron oxides reaches 80–90%, which is confirmed by the data of X-ray diffraction analysis, Mössbauer spectroscopy and magnetometry experiments.

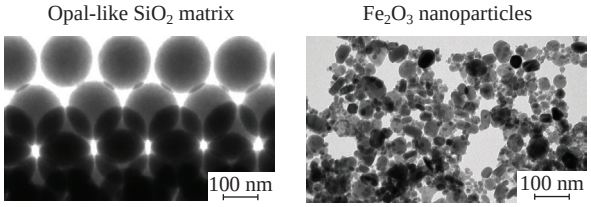

Keywords: ε-Fe_2O_3, nanoparticles, silica, iron oxides, colloid crystals, opal-like matrices, template synthesis.

Currently, five polymorphic modifications of Fe_2O_3 are known: α-Fe_2O_3, β-Fe_2O_3, γ-Fe_2O_3, ε-Fe_2O_3 and ζ-Fe_2O_3.[1] The ε-Fe_2O_3 polymorph occupies a special place among them due to its unique magnetic properties: a very high coercive field (~20 kOe), moderate saturation magnetization and ferroelectricity.[2,3] The presence of such properties makes materials based on ε-Fe_2O_3 promising for the absorption and attenuation of electromagnetic waves in the range of 50–200 GHz, as well as for information storage media.[3–5] Hematite (α-Fe_2O_3) is the thermodynamically most stable form of iron(III) oxide in the macrostate. Stabilization of other modifications of Fe_2O_3 (γ-Fe_2O_3, β-Fe_2O_3 and ε-Fe_2O_3) is possible due to the influence of surface energy in the microstate. The contribution of the surface energy to the total energy of the system depends on the size of the nanoparticles; therefore, different modifications correspond to their own regions of dimensional stability.[6,7] Fe_2O_3 can be obtained by chemical synthesis at relatively low temperatures only in the form of α-Fe_2O_3 and γ-Fe_2O_3 nanoparticles and in the amorphous state.[8] Crystallization of other modifications and polymorphic transformations of Fe_2O_3 require high-temperature (above 600 °C) treatment.[8–10] In this case, aggregation and sintering of nanoparticles lead to the formation of a mixture of Fe_2O_3 polymorphs. Thus, to obtain nanopowders with a high content of one of the modifications, spatial limitation of particle growth is required.

ε-Fe_2O_3 nanoparticles are usually prepared using amorphous silica gel with iron hydroxide inclusions.[11,12] Thermal transformation of precursor nanoparticles (such as α-Fe_2O_3, γ-Fe_2O_3 and Fe_3O_4) of a given size in an inert shell[13–15] or impregnation of mesoporous silica matrices with iron compounds [$FeSO_4$, $Fe(NO_3)_3$ or $Fe(C_{10}H_9CHO)$][16–19] can also be used to obtain nanopowders containing ε-Fe_2O_3. However, all these approaches do not allow one to precisely control the size of the resulting nanoparticles and achieve a high content of ε-Fe_2O_3. Close-packed opal-like structures of spherical SiO_2 particles can be used as an alternative to mesoporous silica gels due to the direct relationship between the diameter of silica particles and the size of voids in a close-packed structure.[20] So, the use of silica particles of different sizes makes it possible to precisely control the size of inorganic nanoparticles obtained in voids of such a structure.

In this work, we investigated the use of close-packed opal-like structures for template synthesis of ε-Fe_2O_3. The effect of matrix properties and heat treatment parameters on the crystallization of iron oxide, the structure and phase composition of iron(III) oxide nanopowders has been established.

Opal-like matrices were obtained by drying a dispersion of monodisperse SiO_2 particles. Then the matrices were impregnated with a solution of iron(III) nitrate, dried at 120 °C and calcined at 200–1100 °C for 2–16 h. Iron(III) nitrate was chosen for impregnation because of its high water solubility and easy thermal decomposition during calcination. For transmission electron microscopy, silicon dioxide was etched with 5 M NaOH solution for 72 h.

As seen in Figure 1(*a*), the resulting matrices are characterized by hexagonal close packing of SiO_2 particles.† When SiO_2 particles larger than 200 nm are used, a bright Bragg color of the matrices is observed, which also confirms the formation of a highly ordered structure. The pore structure of the opal-like matrices was investigated by nitrogen porosimetry.‡ The adsorption isotherms correspond to type IV according to the IUPAC nomenclature, which is characteristic of mesoporous media formed by the packing of spherical particles. The specific surface area was 44 $m^2\ g^{-1}$ for a matrix with SiO_2 particles 100 nm in size. The pore size distribution [Figure 1(*b*)] was calculated from nitrogen adsorption data by the Barrett–Joyner–Halenda method.[21] The main peak in the pore volume distribution near 40 nm corresponds to the octahedral voids of the closest packing.

† Scanning electron microscopy was carried out on a JEOL JSM-6510LV microscope.

‡ Nitrogen porosimetry studies were performed using a Micrometrics ASAP 2020MP adsorption analyzer.

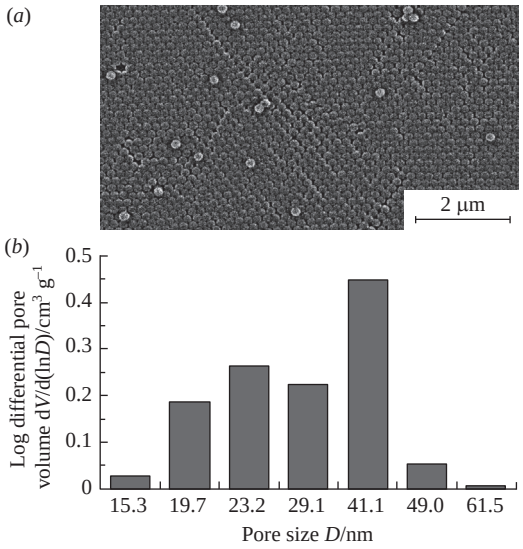

Figure 1 (*a*) Scanning electron microscopy image and (*b*) pore volume distribution of an opal-like matrix of SiO_2 particles.

The second peak near 20 nm corresponds to the tetrahedral voids of the packing. Both peaks are broad and overlap, which is explained by the polydispersity of particles and stacking faults.

Impregnation of the matrix with a solution of iron nitrate leads to a decrease in the volume of mesopores by ~30%, which exceeds the possible degree of filling of mesopores with iron(III) nitrate and its decomposition products. This discrepancy implies blocking a part of the mesopores or supplying an additional amount of iron nitrate from large pores and the surface during the drying process.

In subsequent experiments, matrices with silica particles 110 nm in size were used, considering the pore size distribution and the assumed critical sizes of Fe_2O_3 particles corresponding to various polymorphic modifications.[22] Thermal analysis of the impregnated matrices [Figure 2(*a*)] revealed four major events.[§] The first is manifested by an endothermic peak at about 110 °C, accompanied by a significant weight loss occurring in several stages, mainly associated with the loss of crystallization water of $Fe(NO_3)_3·9H_2O$. The events that caused the second group of peaks at 247 and 310 °C are also expressed in weight loss and are not typical for the decomposition of pure $Fe(NO_3)_3$. These peaks can be associated with the oxidation of organic impurities in the matrix, as well as with partial crystallization of Fe_2O_3 nanoparticles.

The third event with an exothermic peak in the high-temperature region corresponds to the sintering of Fe_2O_3 nanoparticles. Intense sintering occurs in two stages, starting from a temperature of about 450 °C and proceeding most intensively at temperatures above 800 °C. The position of the maximum depends on the heating rate, and at a rate of 25 K min^{-1}, it is at 1150 °C. In the case of sintering pure Fe_2O_3 nanopowders, the process also proceeds in two stages. It also starts at a temperature of about 450 °C, but the second stage of sintering occurs in a narrow temperature range, starting from 730 °C and ending at 800 °C. The kinetic parameters of the observed processes were determined by the Kissinger method. The activation energy of the overall reaction corresponds to 153, 124 and 133 kJ mol^{-1} for the first, second and third peaks, respectively.

To confirm thermal analysis results, we investigated the size of Fe_2O_3 nanoparticles in calcinated samples using transmission electron microscopy [Figure 2(*b*)].[¶] Dependence similar to the

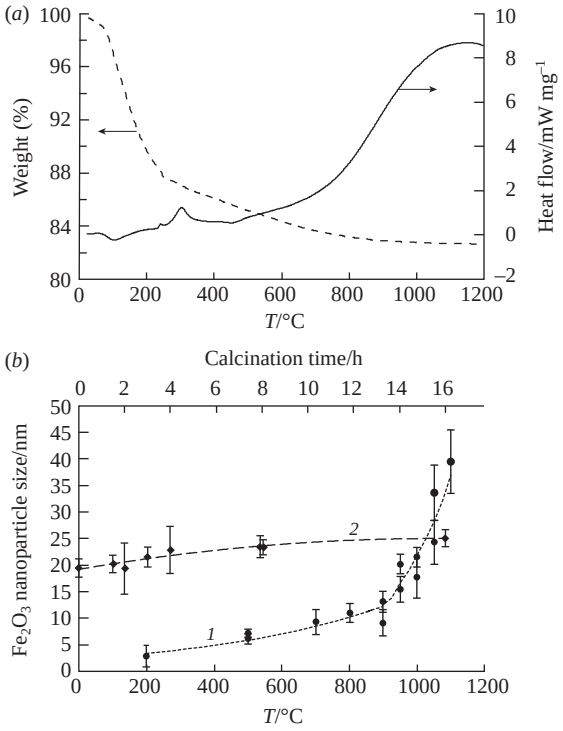

Figure 2 (*a*) Thermal analysis of the impregnated matrix. (*b*) Dependence of the size of Fe_2O_3 nanoparticles on (*1*) temperature and (*2*) duration of calcination.

thermal analysis curve was observed for samples calcined at different temperatures [Figure 2(*b*), curve *1*]. There are regions of crystallization of the initial particles with a smooth increase in size from 3 to 12 nm (up to 900 °C) and sintering of nanoparticles with a sharp increase in size from 12 to 40 nm (above 900 °C). When the samples were calcined at a fixed temperature (1000 °C), the most significant increase in the particle size occurred at the initial stage (4 h) [Figure 2(*b*), curve *2*]. Further calcination (4–16 h) was also accompanied by an increase in the size of nanoparticles, but its rate was about 5 times lower.

Samples obtained at temperatures below 900 °C have small crystallite sizes [Figure 3(*a*)]. In addition, fragments of the pore structure of the matrix can be distinguished. The calcination of samples at temperatures corresponding to the second stage of sintering (above 900 °C) leads to the complete disappearance of the initial structure [Figure 3(*b*)]. There are nanoparticles of three morphologies: small (up to 12 nm) rounded particles, large (more than 40 nm) rounded particles and ellipsoidal particles of intermediate sizes. This diversity can be explained by the presence of nanoparticles of various crystalline modifications of Fe_2O_3, presumably γ-Fe_2O_3 for small isometric particles, α-Fe_2O_3 for large particles and orthorhombic ε-Fe_2O_3 for nanocrystals of intermediate sizes with a characteristic elliptical shape.

It should be noted that the observed change in the microstructure and the coincidence of the temperature of the intensive growth of the size of Fe_2O_3 nanoparticles with the onset temperature of the SiO_2 matrix sintering[23] indicate the predominant role of softening the matrix and an increase in the mobility of matrix particles upon calcining the samples.

The phase composition of the samples was evaluated by X-ray diffraction analysis.[††] Figure 4(*a*) shows a characteristic pattern obtained for a sample calcined at 1000 °C for 3 h. The sample was not purified from SiO_2; therefore, the pattern of the SiO_2 matrix was additionally recorded. The sample contains a large

[§] Synchronous thermal analysis of the obtained samples was conducted on a Netzsch STA 445 Jupiter instrument.

[¶] Transmission electron microscopy studies were conducted on a JEOL JEM-1011 microscope.

[††] Powder X-ray diffraction patterns were obtained on a Bruker D2 Phaser diffractometer using CuKα radiation (λ = 1.540598 Å).

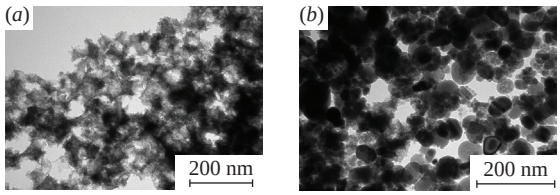

Figure 3 Transmission electron microscopy images of Fe_2O_3 nanoparticles prepared at (*a*) 200 and (*b*) 1050 °C.

fraction of the amorphous phase (broad peak at 20°) corresponding to an amorphous silica matrix. The diffraction pattern shows peaks corresponding to all three modifications of iron(III) oxide, and the predominant modification in all the samples obtained is ε-Fe_2O_3, which causes the most intense reflection in the region of 32° corresponding to the (122) planes of ε-Fe_2O_3.

The XRD results were confirmed by the Mössbauer spectroscopy [Figure 4(*b*)].[‡‡] The observed complex structure can be fitted by a set of a paramagnetic doublet, a relaxation singlet, three sextets corresponding to the three magnetic sublattices of ε-Fe_2O_3 and a sextet corresponding to α-Fe_2O_3. The parameters of the hyperfine structure of the spectra (Table 1) were obtained by the least-squares approximation method with the assumption of a Lorentzian line shape and are in good agreement with the literature data.[24] The partial area of the α-Fe_2O_3 sextet ranges from 2 to 11% for the studied samples. The total partial area of ε-Fe_2O_3 sextets varies in the range of 73–81%. The insignificant (within 2%) paramagnetic doublet is explained by superparamagnetic Fe_2O_3 nanoparticles less than 2 nm in size. The remaining area belongs predominantly to a broad relaxation 'Lorentzian' singlet. This singlet may be due to the presence of very small superparamagnetic particles of γ-Fe_2O_3, ε-Fe_2O_3 or both, ranging in size from 2 to 4 nm.

γ-Fe_2O_3 and ε-Fe_2O_3 nanopowders have significantly different values of saturation magnetization (about 80 and 12 A m kg^{-1}, respectively), which makes it possible to distinguish them using magnetometric measurements. The field dependences of nanopowders obtained by calcining impregnated matrices have been investigated.[§§] It was shown that with increasing particle size, a monotonic decrease in magnetization is observed due to a decrease in the γ-Fe_2O_3 content. The coercive field at room temperature was 12.5 kOe for samples obtained in matrices with SiO_2 particles 110 nm in size. The obtained value of the coercive field agrees well with the assumption of the random orientation of ε-Fe_2O_3 nanoparticles.

The use of opal-like structures of silicon dioxide as a template for the synthesis of iron(III) oxide nanoparticles makes it possible to effectively control the phase composition of the resulting nanopowders. The maximum content of ε-Fe_2O_3 is achieved at a matrix particle size of 100–110 nm. The optimal conditions for

Table 1 Parameters of the hyperfine structure of Mössbauer spectra.

Subspectrum	Partial area (%)	Isomer shift/ mm s^{-1}	Quadrupole splitting/mm s^{-1}	Hyperfine field B_{hf}/T
α-Fe_2O_3	2	0.38	−0.22	51.2
ε-Fe_2O_3-1	33	0.37	−0.23	44.7
ε-Fe_2O_3-2	28	0.37	−0.03	39.2
ε-Fe_2O3-3	19	0.19	−0.16	26.1
Singlet	15	0.26	0.00	0.0
Doublet	3	0.43	0.86	0.0

[‡‡] Mössbauer spectra were recorded on an MS-1104Em spectrometer operating in the constant-acceleration mode with the ^{57}Co isotope in a rhodium matrix as a source of resonant gamma radiation.

[§§] Magnetic measurements were carried out on a Quantum Design SQUID magnetometer.

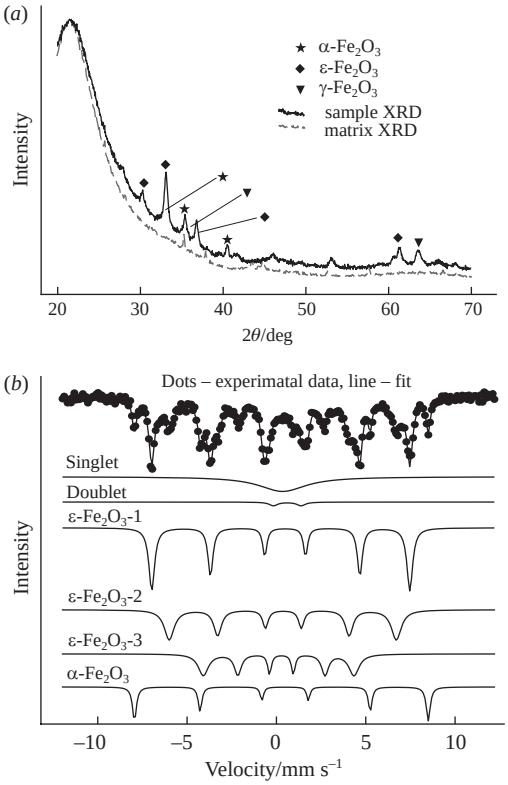

Figure 4 (*a*) X-ray diffraction patterns and (*b*) ^{57}Fe Mössbauer spectrum of a sample calcined at 1000 °C for 3 h.

the synthesis of ε-Fe_2O_3 nanoparticles in opal-like matrices are calcination at a temperature of 1000 °C for 2–4 h. The fraction of ε-Fe_2O_3 in mixtures of iron oxide modifications reaches 80–90%, which is confirmed by the data of X-ray diffraction analysis and Mössbauer spectroscopy. The results obtained make it possible to predict the phase composition of nanopowders obtained by this method and can be used to obtain nanostructured, including opal-like, materials based on ε-Fe_2O_3.

This work was supported by the Russian Foundation for Basic Research (project no. 20-03-00668). Scanning electron microscopy and nitrogen porosimetry studies were conducted on facilities of D. I. Mendeleev Resource Sharing Center.

References

1 L. Machala, J. Tuček and R. Zbořil, *Chem. Mater.*, 2011, **23**, 3255.
2 J. Jin, S. Ohkoshi and K. Hashimoto, *Adv. Mater.*, 2004, **16**, 48.
3 J. Tuček, R. Zbořil, A. Namai and S. Ohkoshi, *Chem. Mater.*, 2010, **22**, 6483.
4 A. Namai, S. Sakurai, M. Nakajima, T. Suemoto, K. Matsumoto, M. Goto, S. Sasaki and S. Ohkoshi, *J. Am. Chem. Soc.*, 2009, **131**, 1170.
5 S. Ohkoshi, S. Kuroki, S. Sakurai, K. Matsumoto, K. Sato and S. Sasaki, *Angew. Chem., Int. Ed.*, 2007, **46**, 8392.
6 S. Lee and H. Xu, *J. Phys. Chem. C*, 2016, **120**, 13316.
7 S. Sakurai, A. Namai, K. Hashimoto and S. Ohkoshi, *J. Am. Chem. Soc.*, 2009, **131**, 18299.
8 E. E. Yurmanova, I. M. Le-Deygen, V. V. Spiridonov and A. V. Sybachin, *Mendeleev Commun.*, 2020, **30**, 768.
9 P. Brázda, E. Večerníková, E. Pližingrová, A. Lančok and D. Nižňanský, *J. Therm. Anal. Calorim.*, 2014, **117**, 85.
10 M. Gich, A. Roig, E. Taboada, E. Molins, C. Bonafos and E. Snoeck, *Faraday Discuss.*, 2007, **136**, 345.
11 J. López-Sánchez, A. Muñoz-Noval, A. Serrano, M. Abuín, J. de la Figuera, J. F. Marco, L. Pérez, N. Carmona and O. Rodríguez de la Fuente, *RSC Adv.*, 2016, **6**, 46380.
12 K. C. Barick, B. S. D. Ch. S. Varaprasad and D. Bahadur, *J. Non-Cryst. Solids*, 2010, **356**, 153.
13 M. Tadić, V. Spasojević, V. Kusigerski, D. Marković and M. Remškar, *Scr. Mater.*, 2008, **58**, 703.
14 E. Taboada, M. Gich and A. Roig, *ACS Nano*, 2009, **3**, 3377.

15 M. Nakaya, R. Nishida, N. Hosoda and A. Muramatsu, *Cryst. Res. Technol.*, 2017, **52**, 1700110.
16 E. Delahaye, V. Escax, N. El Hassan, A. Davidson, R. Aquino, V. Dupuis, R. Perzynski and Y. L. Raikher, *J. Phys. Chem. B*, 2006, **110**, 26001.
17 L. Kubíčková, J. Kohout, P. Brázda, M. Veverka, T. Kmječ, D. Kubániová, P. Bezdička, M. Klementová, E. Šantavá and K. Závěta, *Hyperfine Interact.*, 2016, **237**, 159.
18 S. Ohkoshi, A. Namai and S. Sakurai, *J. Phys. Chem. C*, 2009, **113**, 11235.
19 A. A. Shesterkina, E. V. Shuvalova, E. A. Redina, O. A. Kirichenko, O. P. Tkachenko, I. V. Mishin and L. M. Kustov, *Mendeleev Commun.*, 2017, **27**, 512.
20 T. Aste and D. Weaire, *The Pursuit of Perfect Packing*, 2nd edn., CRC Press, Boca Raton, FL, 2008.
21 E. P. Barrett, L. G. Joyner and P. P. Halenda, *J. Am. Chem. Soc.*, 1951, **73**, 373.
22 A. I. Sharapaev, S. A. Kuznetsova, A. N. Norenko, A. G. Muradova, N. P. Simonenko and E. V. Yurtov, *Russ. J. Inorg. Chem.*, 2021, **66**, 740 (*Zh. Neorg. Khim.*, 2021, **66**, 641).
23 B. Topuz, D. Şimşek and M Çiftçioğlu, *Ceram. Int.*, 2015, **41**, 43.
24 P. Brázda, D. Nižňanský, J.-L. Rehspringer and J. Poltierová Vejpravová, *J. Sol-Gel Sci. Technol.*, 2009, **51**, 78.

Received: 11th October 2021; Com. 21/6722